DEUTSCHES ELEKTRONEN – SYNCHROTRON

DESY 92-146
October 1992

Investigation of the Decays $\overline{B}^0 \to D^{*+}\ell^-\overline{\nu}$ and $\overline{B} \to D^{**}\ell^-\overline{\nu}$

The ARGUS Collaboration

ISSN 0418-9833

NOTKESTRASSE 85 · D-2000 HAMBURG 52

To be sure that your preprints are promptly included in the
HIGH ENERGY PHYSICS INDEX,
send them to (if possible by air mail):

DESY
Bibliothek
Notkestraße 85
W-2000 Hamburg 52
Germany

DESY-IfH
Bibliothek
Platanenallee 6
O-1615 Zeuthen
Germany

DESY 92-146
October 1992

ISSN 0418-9833

Investigation of the Decays $\overline{B}^0 \to D^{*+}\ell^-\overline{\nu}$ and $\overline{B} \to D^{**}\ell^-\overline{\nu}$

The ARGUS Collaboration

H. Albrecht, H. Ehrlichmann, T. Hamacher, R. P. Hofmann, T. Kirchhoff, A. Nau, S. Nowak[1], H. Schröder, H. D. Schulz, M. Walter[1], R. Wurth
DESY, Hamburg, Germany

R. D. Appuhn, C. Hast, H. Kolanoski, A. Lange, A. Lindner, R. Mankel, M. Schieber, T. Siegmund, B. Spaan, H. Thurn, D. Töpfer, A. Walther, D. Wegener
Institut für Physik[2], Universität Dortmund, Germany

M. Bittner, P. Eckstein
Institut für Kern- und Teilchenphysik[3], Technische Universität Dresden, Germany

M. Paulini, K. Reim, H. Wegener
Physikalisches Institut[4], Universität Erlangen-Nürnberg, Germany

R. Mundt, T. Oest, R. Reiner, W. Schmidt-Parzefall
II. Institut für Experimentalphysik, Universität Hamburg, Germany

W. Funk, J. Stiewe, S. Werner
Institut für Hochenergiephysik[5], Universität Heidelberg, Germany

K. Ehret, W. Hofmann, A. Hüpper, S. Khan, K. T. Knöpfle, J. Spengler
Max-Planck-Institut für Kernphysik, Heidelberg, Germany

D. I. Britton[6], C. E. K. Charlesworth[7], K. W. Edwards[8], E. R. F. Hyatt[6], H. Kapitza[8], P. Krieger[9,7], D. B. MacFarlane[6], P. M. Patel[6], J. D. Prentice[7], P. R. B. Saull[6], K. Tzamariudaki[6], R. G. Van de Water[7], T.-S. Yoon[7]
Institute of Particle Physics[10], Canada

D. Reßing, M. Schmidtler, M. Schneider, K. R. Schubert, K. Strahl, R. Waldi, S. Weseler
Institut für Experimentelle Kernphysik[11], Universität Karlsruhe, Germany

G. Kernel, P. Križan, E. Križnič, T. Podobnik, T. Živko
Institut J. Stefan and Oddelek za fiziko[12], Univerza v Ljubljani, Ljubljana, Slovenia

V. Balagura, I. Belyaev, S. Chechelnitsky, M. Danilov, A. Droutskoy, Yu. Gershtein, A. Golutvin, I. Gorelov, G. Kostina, V. Lubimov, P. Pakhlov, F. Ratnikov, S. Semenov, V. Shibaev, V. Soloshenko, I. Tichomirov, Yu. Zaitsev
Institute of Theoretical and Experimental Physics, Moscow, Russia

[1] DESY, IfH Zeuthen

[2] Supported by the German Bundesministerium für Forschung und Technologie, under contract number 054DO51P.
[3] Supported by the German Bundesministerium für Forschung und Technologie, under contract number 055DD11P.
[4] Supported by the German Bundesministerium für Forschung und Technologie, under contract number 054ER12P.
[5] Supported by the German Bundesministerium für Forschung und Technologie, under contract number 055HD21P.
[6] McGill University, Montreal, Quebec, Canada.
[7] University of Toronto, Toronto, Ontario, Canada.
[8] Carleton University, Ottawa, Ontario, Canada.
[9] Supported in part by the Walter C. Sumner Foundation.
[10] Supported by the Natural Sciences and Engineering Research Council, Canada.
[11] Supported by the German Bundesministerium für Forschung und Technologie, under contract number 054KA17P.
[12] Supported by the Department of Science and Technology of the Republic of Slovenia and the Internationales Büro KfA, Jülich.

Abstract

Exclusive semileptonic B decays with a D^{*+} meson in the final state have been studied using the ARGUS detector at the DORIS II storage ring. The branching ratio for the decay $\overline{B}^0 \to D^{*+}\ell^-\overline{\nu}$, where ℓ^- is either e^- or μ^-, has been measured to be $(5.2 \pm 0.5 \pm 0.6)\%$. A significant rate for the decay $\overline{B} \to D^{**}\ell^-\overline{\nu}$ has been observed. From an angular analysis of the cascade $\overline{B}^0 \to D^{*+}(\to D^0\pi^+)\ell^-\overline{\nu}$ the forward-backward asymmetry A_{FB} and the D^{*+} polarization parameter α have been determined to be $A_{FB} = 0.20 \pm 0.08 \pm 0.06$ and $\alpha = 1.1 \pm 0.4 \pm 0.2$.

1 Introduction

The well-known exclusive semileptonic decay[1] $\overline{B}^0 \to D^{*+}\ell^-\overline{\nu}$ has recently gained new importance as a means of determining the CKM matrix element $|V_{cb}|$ and for testing the Lorentz structure of the weak hadronic current. The study of this channel was pioneered by ARGUS in 1987 [1]. Among its advantages is the fact that it has the largest single branching ratio for B decays ($4.9 \pm 0.8\%$ [2]) which, together with an efficiency times branching ratio for the accessible charm channels of more than 1%, results in statistically favourable reconstructed data samples. In addition, the background for this decay is relatively small and well understood. These considerations have allowed us to use this channel for detailed tests of theoretical models and their internal consistency.

Over the last few years great progress has been made in our understanding of exclusive semileptonic decays, both in the context of Heavy Quark Effective Theory (HQET) [3, 4] and using QCD sum rules [5]. For the HQET approach it has been shown that the decay $\overline{B}^0 \to D^{*+}\ell^-\overline{\nu}$ is not affected by $O(1/m_Q)$ corrections at the point of zero recoil, i.e. at the maximum momentum transfer $q^2 = q^2_{max}$ [6]. The q^2 spectrum for the decay $\overline{B}^0 \to D^{*+}\ell^-\overline{\nu}$ is hard due to the spin $J = 1$ of the D^{*+} meson. In principle, this allows a model independent determination of $|V_{cb}|$ from the study of the q^2 spectrum. Furthermore, the decay $\overline{B}^0 \to D^{*+}\ell^-\overline{\nu}$ allows one to measure the chirality of the weak b to c transition [7], which is only possible if the daughter meson has spin $J > 0$.

The decay $\overline{B}^0 \to D^{*+}\ell^-\overline{\nu}$ followed by $D^{*+} \to D^0\pi^+$ is completely described by specifying q^2 and the three angular degrees of freedom defined in Fig. 1. Neglecting the masses of the e^- and μ^-, the differential decay width can be written as:

$$\frac{d^4\Gamma(q^2, \cos\theta, \cos\theta^*, \chi)}{dq^2\, d\cos\theta\, d\cos\theta^*\, d\chi} = \mathrm{Br}(D^{*+} \to D^0\pi^+)\frac{G_F^2}{(2\pi)^3}|V_{cb}|^2\frac{q^2 p}{12M^2_{\overline{B}^0}} \times \left|\sum_\lambda d^1_{0,\lambda}(\theta^*)\cdot d^1_{\lambda,1}(\theta)\cdot e^{-i(\lambda+1)\chi}\cdot H_\lambda(q^2)\right|^2 \quad (1)$$

[1] Unless otherwise stated references in this paper to a specific charged state are to be interpreted as implying the charge-conjugate state as well.

where p is the D^{*+}-momentum in the $\overline{B}^0$ rest frame and $H_\lambda(q^2)$ are the helicity form factors. One qualitatively expects $|H_-|^2 > |H_+|^2$ since the c-quark in the D^{*+}-meson is produced with predominantly negative helicity, and both helicities occur with equal amplitude for the spectator $\bar{d}$-quark. Hence, parity violation in the weak interaction should manifest itself as a forward-backward asymmetry A_{FB} in the distribution of $\cos\theta$ [8]:

$$\frac{d\Gamma(\cos\theta)}{d\cos\theta} \propto \alpha \cdot \sin^2\theta - \frac{4}{3}A_{FB}(3+\alpha)\cdot\cos\theta + 2 \qquad (2)$$

where

$$A_{FB} = \frac{\int_{-1}^{0}\frac{d\Gamma(\cos\theta)}{d\cos\theta}d\cos\theta - \int_{0}^{+1}\frac{d\Gamma(\cos\theta)}{d\cos\theta}d\cos\theta}{\int_{-1}^{+1}\frac{d\Gamma(\cos\theta)}{d\cos\theta}d\cos\theta} = \frac{3}{4}\cdot\frac{\Gamma_- - \Gamma_+}{\Gamma}. \qquad (3)$$

The helicity alignment of the W^- is given by $\alpha = 2\Gamma^0/(\Gamma^+ + \Gamma^-) - 1$, which describes the D^{*+} polarization extracted from the D^{*+} decay angle distribution via:

$$\frac{d\Gamma(\cos\theta^*)}{d\cos\theta^*} \propto 1 + \alpha\cdot\cos^2\theta^*. \qquad (4)$$

The theoretical predictions for A_{FB} depend on model calculations of the invariant form factors F_1^A, F_2^A, and F^V, which are related to the helicity form factors by:

$$\begin{aligned} H_0(q^2) &= \frac{1}{2M_{D^{*+}}\sqrt{q^2}}\left[\left(M_{\overline{B}^0}^2 - M_{D^{*+}}^2 - q^2\right)F_1^A(q^2) + 2M_{\overline{B}^0}^2 p^2 F_2^A(q^2)\right] \\ H_\pm(q^2) &= F_1^A(q^2) \pm M_{\overline{B}^0} p F^V(q^2). \end{aligned} \qquad (5)$$

There exist a number of form factor predictions, based on quark model wave functions and single-pole dominance [8–12], which lead to values for A_{FB} in the range from 0.15 to 0.20. Recent QCD-sum rule calculations [5] of the invariant form factors yield a larger value of $A_{FB} = 0.23$.

2 Data Sample and Concepts

The data used in this analysis were collected with the ARGUS detector at the DORIS II storage ring over the period 1983 to 1990. At the energy of the $\Upsilon(4S)$ an integrated luminosity of 233 pb^{-1} has been collected. This corresponds to $(1.98 \pm 0.10)\times 10^5$ $B\overline{B}$ pairs, assuming the $\Upsilon(4S)$ resonance decays only into B mesons. Background from non-resonant e^+e^- annihilation into $q\bar{q}$ pairs is studied with a continuum data sample corresponding to an integrated luminosity of about 105 pb^{-1} recorded in the energy range from 10.432 GeV to 10.548 GeV. Details concerning the ARGUS detector, the trigger system, and the reconstruction and particle identification capabilities can be found in [13].

To study semileptonic decays of B-mesons we select events containing at least one electron or muon with momentum greater than 1 GeV/c. Lepton identification was based

on an electron- or muon-specific likelihood ratio formed by combining the measurements of specific ionization dE/dx, time-of-flight, size and shape of the energy deposition in the electromagnetic calorimeter, and hits in the muon chambers. For both the electron and muon hypotheses the appropriate likelihood ratio is required to be larger than 0.7. The polar angle θ of the lepton momentum with respect to the beam axis is required to lie in the interval $|\cos\theta| < 0.85$.

D^{*+} mesons are reconstructed in the two decay chains $D^{*+} \to D^0\pi^+$ with $D^0 \to K^-\pi^+$ and $D^0 \to K^-\pi^+\pi^+\pi^-$. In Fig. 2 we show the spectrum of invariant $(D^0\pi^+)$ mass for the two D^0 channels. These distributions include only $(D^0\pi^+)$-combinations in events containing a negatively-charged lepton where the reconstructed D^0 mass lies within $\pm 60\,\mathrm{MeV}/c^2$ of the nominal D^0 mass [2]. We furthermore required $x_p := p_{D^{*+}}/\sqrt{E_{beam}^2 - M_{D^{*+}}^2} < 0.5$ which is the kinematically allowed range for a D^{*+} meson in a B decay. The number of $(D^{*+}\ell^-)$ pairs is determined by fitting a Gaussian distribution for the signal above a combinatorial background. The shape of this background varies widely, depending on whether or not some of the actual decay products from the D^{*+} are retained in combination with other uncorrelated hadrons in the event. The different background shapes have been determined by a Monte Carlo simulation. The total background rate is obtained by fitting a linear combination of the various contributions. This procedure, applied bin-by-bin, has been used in order to derive the M_{rec}^2, q^2, $\cos\theta$, $\cos\theta^*$, and $M(D^{*+}\pi^-)$ distributions described below.

On the $\Upsilon(4S)$, events with $(D^{*+}\ell^-)$ pairs arise from the four different sources listed in Tab. 1. They consist of the channel $\overline{B}^0 \to D^{*+}\ell^-\overline{\nu}$ (I), which is the main concern of this analysis, and backgrounds from processes (II-IV). Of some interest in its own right is the decay $\overline{B} \to D^{**}\ell^-\overline{\nu}$ (II), which will be the subject of a specific study described below.

The signal for the reaction $\overline{B}^0 \to D^{*+}\ell^-\overline{\nu}$ (I) is obtained from the distribution of the recoil-mass squared:

$$M_{rec}^2 = (E_{beam} - E_{D^{*+}} - E_{\ell^-})^2 - (\vec{p}_{D^{*+}} + \vec{p}_{\ell^-})^2. \qquad (6)$$

For reaction I M_{rec}^2 is approximately the neutrino rest mass squared M_ν^2, since the $\overline{B}^0$ momentum is small.

The M_{rec}^2 distribution for the decay $\overline{B}^0 \to D^{*+}\ell^-\overline{\nu}$ has been obtained from Monte Carlo studies based on [5,8–12]. The distributions obtained from the various models are very similar. They are represented in Fig. 3 by the one curve which peaks at $M_{rec}^2 = 0$. For the background process $\overline{B} \to D^{**}\ell^-\overline{\nu}$ (II) we apply the GISW model [10]. The predictions for the D^{**} resonances, with quantum numbers $n^{(2S+1)}L_J = \{1^1P_1, 1^3P_{1,2}, 2^1S_0, 2^3S_1\}$, are accounted for in estimating the contributions to the $D^{*+}\pi$ final state. Note that the 1^3P_0 state is excluded, for which a decay into $D^{*+}\pi^-$ is prohibited by angular momentum and parity conservation. The contribution from background process II is shifted to positive

M^2_{rec} values as expected from the non-vanishing $(\overline{\nu}\,\pi)$ invariant mass. Fig. 3 also includes the M^2_{rec}-distributions for cases where the D^{*+} and the ℓ^- are produced in different B decays (III) or in non-resonant e^+e^- annihilation (IV). These were obtained respectively from Monte Carlo simulations of $B\overline{B}$ events [14] and continuum e^+e^- processes generated using the JETSET 6.3 version of the LUND model [15].

3 Results

3.1 Branching Ratio for the Decay $\overline{B}^0 \to D^{*+}\,\ell^-\,\overline{\nu}$

Fig. 4 a,b show the measured M^2_{rec} distribution for the two decay chains $D^{*+} \to D^0\,\pi^+$, followed by $D^0 \to K^-\,\pi^+$ and $D^0 \to K^-\,\pi^+\,\pi^+\,\pi^-$, respectively. In both cases a prominant signal at $M^2_{rec} = 0$ is observed, as expected for the decay $\overline{B}^0 \to D^{*+}\,\ell^-\,\overline{\nu}$. The small number of events at $M^2_{rec} < -2\,\mathrm{GeV}^2/c^4$ indicates that there are only minor backgrounds from processes III (uncorrelated $D^{*+}\,\ell^-$) and IV (continuum). Hadron misidentification as an electron or muon can only occur for these particular sources, and has been accounted for in estimating their contribution.

For positive M^2_{rec} values one observes a shoulder which is attributed to the process $\overline{B} \to D^{**}\,\ell^-\,\overline{\nu}$ (II). From a fit to the M^2_{rec} distribution which uses the shapes shown in Fig. 3, the event rates listed in Tab. 2 are obtained. The rate for the continuum process (IV) has been constrained to the number of $(D^{*+}\ell^-)$ pairs in the continuum data sample where we observe 2.6 ± 1.8 and 6.2 ± 4.8 $(D^{*+}\,\ell^-)$ combinations for the two decay chains respectively. These measured number of events are then scaled by a factor of 2.2 in order to account for the ratio of the integrated luminosities and the hadronic cross section.

The fitted number of $(D^{*+}\,\ell^-)$ events for the process $\overline{B}^0 \to D^{*+}\,\ell^-\,\overline{\nu}$ given in Tab. 2 lead to branching ratios of $(5.5\pm0.6\pm0.7)\%$ and $(4.7\pm0.9\pm0.5)\%$ for the two decay chains respectively. In obtaining this result, the relevant charm branching ratios $\mathrm{Br}(D^{*+} \to D^0\,\pi^-) = 68.1\%$ [16], $\mathrm{Br}(D^0 \to K^-\,\pi^+) = 3.65\%$ [2], and $\mathrm{Br}(D^0 \to K^-\,\pi^+\,\pi^+\,\pi^-) = 7.5\%$ [2] have been used. Assuming lepton universality, the measurements can be combined to give:

$$\mathrm{Br}(\overline{B}^0 \to D^{*+}\,\ell^-\,\overline{\nu}) = (5.2 \pm 0.5 \pm 0.6)\%.$$

This value replaces the previous ARGUS result [1] and is in agreement with other measurements [2]. The second error is due to systematic uncertainties, and includes the variation of the result using the different available models to describe process I [5,8–12] and process II with D^{**} quantum numbers 1^1P_1, $1^3P_{1,2}$, 2^1S_0, and 2^3S_1 [10]. The systematic errors also cover the uncertainty in the parametrization of the combinatorial background under the D^{*+} signal which has been studied by varying the D^0 mass cuts.

3.2 Observation of the Decay $\overline{B} \to D^{**}\,\ell^-\,\overline{\nu}$

The fitted rate of $63 \pm 15 \pm 6$ candidates for process II given in Tab. 2 establishes a significant contribution for D^{**} production in semileptonic B decays. In order to provide further confirmation of this result, the invariant mass distribution of $(D^{*+}\,\pi^-)$ combinations has been studied. For this purpose the data sample is split into two parts: one for positive M^2_{rec}, where resonances in the invariant $(D^{**}\,\pi^-)$ mass can be expected, and the other for negative M^2_{rec}, where a contribution from D^{**} resonances can be neglected, as can be seen from distribution II of Fig. 3. The sample for negative M^2_{rec} is therefore used to determine the combinatorial background in the sample for positive M^2_{rec}. Since the combinatorial background in the $(D^{*+}\,\pi^-)$ mass distribution scales like the number of $(D^{*+}\,\ell^-)$ pairs, the ratio of the level of combinatorial background in the two samples is known. Shown in Fig. 5 are the invariant mass spectrum $M(D^{*+}\,\pi^-)$ for both $M^2_{rec} > 0$ and $M^2_{rec} < 0$. The distribution for $M^2_{rec} > 0$ shows an enhancement at the mass of the known P-wave D mesons. The distribution for $M^2_{rec} < 0$ has been scaled to correspond to the combinatorial background in the first distribution. Both distributions are simultaneously fit with the same background shape, parametrized by the product of a threshold factor with an exponential times second-order polynomial. In addition, for the sample with $M^2_{rec} > 0$, the fit function includes two Breit-Wigner resonances to allow for contributions from P-wave states with masses of 2420 and 2460 MeV/c^2 and full widths of 20 MeV/c^2, as previously determined from inclusive measurements [17]. From the fit, a signal of 30 ± 10 D^{**0} events is determined for the sum of contributions from both resonances. This number should be compared to the $63 \pm 15 \pm 6$ $(D^{*+}\ell^-)$ combinations extracted from the fit to the M^2_{rec} distribution. The level of the expected signal for P-wave mesons must account for the fact that only 2/3 of the D^{*+} mesons are due to the decay $D^{**0} \to D^{*+}\pi^-$ by isospin arguments and the detection efficiency for the additional charged pion is only 84%. Hence, we estimate that 35 ± 9 D^{**0} mesons should be reconstructed, in excellent agreement with the fit result. The observation of a shoulder in the M^2_{rec} spectrum at positive values which is backed up by an enhancement in the $D^{*+}\pi^-$ spectrum at the mass of the known P-wave D mesons is the first direct evidence for D^{**} production in semileptonic B decays.

The ratio $N(D^{**}\ell^-)/N(D^{*+}\ell^-) = 0.27 \pm 0.08 \pm 0.03$ extracted from the M^2_{rec} distributions and the branching ratio $\mathrm{Br}(\overline{B}^0 \to D^{*+}\,\ell^-\,\overline{\nu}) = (5.2 \pm 0.5 \pm 0.6)\%$ (see Tab. 2) can be used to estimate the branching ratio $\mathrm{Br}(\overline{B}^0 \to D^{**+}\,\ell^-\,\overline{\nu})$. The relation between these two quantities is given by:

$$\frac{N(D^{**}\ell^-)}{N(D^{*}\ell^-)} = \frac{\sum_i \{\ \mathrm{Br}(B^- \to D_i^{**0}\,\ell^-\,\overline{\nu}) \cdot \mathrm{Br}(D_i^{**0} \to D^{*+}\,\pi^-) \cdot N_{B^-} \\ +\ \mathrm{Br}(\overline{B}^0 \to D_i^{**+}\,\ell^-\,\overline{\nu}) \cdot \mathrm{Br}(D_i^{**+} \to D^{*+}\,\pi^0) \cdot N_{\overline{B}^0}\ \} \cdot \epsilon_i^{**}}{\mathrm{Br}(\overline{B}^0 \to D^{*+}\,\ell^-\,\overline{\nu}) \cdot N_{\overline{B}^0}}, \qquad (7)$$

where ϵ_i^{**} denotes the efficiency for accepting a $(D^{*+}\,\ell^-)$ pair due to a B-decay via a D^{**}

meson of type $i = \{1^1P_1,\ 1^3P_{1.2},\ 2^1S_0,\ 2^3S_1\}$, divided by the corresponding efficiency for process I. We use the following assumptions to simplify equation (7):

- $N_{B^-} = N_{\overline{B}^0}$
- $\mathrm{Br}(B^- \to D_i^{**0}\,\ell^-\,\bar{\nu}) \approx \mathrm{Br}(\overline{B}^0 \to D_i^{**+}\,\ell^-\,\bar{\nu})$
- $\frac{1}{2}\cdot\mathrm{Br}(D_i^{**0} \to D^{*+}\,\pi^-) = \mathrm{Br}(D_i^{**+} \to D^{*+}\,\pi^0) = \frac{1}{3}\cdot\mathrm{Br}(D_i^{**+} \to D^*\,X)$.

The last relation is motivated from isospin considerations where the decay $D_i^{**} \to D^{*+}X$ is assumed to be saturated with $X = \pi^0/\pi^-$, i.e. neglecting radiative or multi-pion decays of the D^{**} mesons. Inserting $\mathrm{Br}(\overline{B}^0 \to D^{**+}\ell^-\bar{\nu}) = \sum_i \mathrm{Br}(\overline{B}^0 \to D_i^{**+}\ell^-\bar{\nu})$ leads to the following relation between the ratio of observed numbers of $(D^*\ell^-)$ pairs due to process II and I and the ratio of corresponding $\overline{B}^0$ branching ratios:

$$\frac{N(D^{**}\ell^-)}{N(D^*\ell^-)} = \frac{\mathrm{Br}(\overline{B}^0 \to D^{**+}\ell^-\bar{\nu})}{\mathrm{Br}(\overline{B}^0 \to D^{*+}\ell^-\bar{\nu})} \cdot \frac{\sum_i\{\mathrm{Br}(\overline{B}^0 \to D_i^{**+}\ell^-\bar{\nu})\cdot\mathrm{Br}(D_i^{**+} \to D^*X)\cdot\varepsilon_i^{**}\}}{\sum_i \mathrm{Br}(\overline{B}^0 \to D_i^{**+}\ell^-\bar{\nu})}.$$

The second ratio on the right hand side of this equation must be determined from theoretical predictions. It contains three quantities for each type of D^{**} resonance which are listed in Tab. 3. Using the results from the GISW model [10] we obtain a value of 0.52 for this ratio, leading to

$$\mathrm{Br}(\overline{B}^0 \to D^{**+}\ell^-\bar{\nu}) = (2.7 \pm 0.5 \pm 0.5)\%.$$

Calculating the numbers ε_i^{**} from the BHKT model[2] [4] we obtain

$$\mathrm{Br}(\overline{B}^0 \to D^{**+}\ell^-\bar{\nu}) = (2.3 \pm 0.6 \pm 0.4)\%.$$

This result implies a significant contribution from D^{**} mesons in semileptonic B decays and solves a long-standing problem that the inclusive semileptonic rate was not saturated by the decays $\overline{B} \to D\,\ell^-\bar{\nu}$ and $\overline{B} \to D^*\,\ell^-\,\bar{\nu}$. Summing up the branching ratios for the exclusive semileptonic B decays into D^*, D^{**} and D mesons, where for the latter we use the ARGUS measurement of $(1.9 \pm 0.6 \pm 0.5)\%$ [18], we find

$$\mathrm{Br}(\overline{B} \to (D, D^*, D^{**})\ell^-\bar{\nu}) = (9.4\text{–}9.8) \pm 1.0 \pm 0.9\%$$

in good agreement with the total inclusive branching ratio and the small value of the coupling for $b \to u$ transitions.

[2] We apply the Isgur-Wise-Functions $\xi_{1/2}^*(y) \propto [1 + \frac{1}{2}(y-1)]^{-2}$ and $\xi_{3/2}^*(y) \propto [1 + \frac{1}{2}(y-1)]^{-3}$.

3.3 Measurement of the Forward-Backward Asymmetry A_{FB}

The Lorentz structure of the decay $\overline{B}^0 \to D^{*+}\,\ell^-\,\bar{\nu}$ has been studied by extracting the differential decay widths as a function of $\cos\theta$, $\cos\theta^*$, and q^2. These distributions are produced by requiring that the momenta and energies of the D^{*+} and the ℓ^- be consistent with the presumed decay of a $\overline{B}^0$ meson. Specifically, the neutrino energy $E_{\bar{\nu}} = E_{beam} - E_{D^{*+}} - E_{\ell^-}$ must be positive, and the neutrino momentum $p_{\bar{\nu}} = E_{\bar{\nu}}$, together with the known $p_{\overline{B}^0} = \sqrt{E_{beam}^2 - M_{\overline{B}^0}^2}$ and $p_{D^{*+}\ell^-} = |\vec{p}_{D^{*+}} + \vec{p}_{\ell^-}|$, must be consistent with momentum conservation, i.e. form a closed momentum triangle. These conditions are fulfilled only for $(D^{*+}\,\ell^-)$ pairs with $M_{rec}^2 \approx 0$, and therefore automatically select the decay $\overline{B}^0 \to D^{*+}\,\ell^-\,\bar{\nu}$, while considerably reducing the background. Fig. 6 shows the $\cos\theta$, $\cos\theta^*$, q^2, and the M_{rec}^2 distributions obtained under these conditions without applying efficiency corrections. The $\cos\theta$ spectrum exhibits a strong fall-off as $\cos\theta$ approaches $+1$. This is mainly a kinematic effect due to the cut on the lepton momentum, $p_l > 1\,\mathrm{GeV}/c$.

The four distributions in Fig. 6 are fitted again on the basis of the models [5,8–12] for the process $\overline{B}^0 \to D^{*+}\,\ell^-\,\bar{\nu}$ and [10] for $\overline{B} \to D^{**}\,\ell^-\,\bar{\nu}$. For the latter process the joint angular decay distribution for the whole cascade $\bar{B} \to D^{**}[\to D^*(\to D\,\pi)]\,l\,\nu$ has been worked out [19]. To determine the forward-backward asymmetry A_{FB} and the polarization parameter α, the normalizations of the three invariant form factors in each model (see eq. 5) are varied to simultaneously fit all four differential distributions. The background rate in the $\cos\theta$, $\cos\theta^*$, and q^2 distributions due to processes II through IV is determined from the M_{rec}^2 spectrum. A_{FB} and α are calculated by inserting the adjusted normalizations of the invariant form factors into eq. (1). A check was made to demonstrate that such a procedure is not biased by the model used for the form factors. The method has the advantage that the value determined for A_{FB} and α is independent of the cut on the lepton momentum. The simultaneous fit yields (see Tab. 2):

$$A_{FB} = \frac{3}{4}\cdot\frac{\Gamma^- - \Gamma^+}{\Gamma} = 0.20 \pm 0.08 \pm 0.06$$

and

$$\alpha = 2\cdot\frac{\Gamma^L}{\Gamma^T} - 1 = 1.1 \pm 0.4 \pm 0.2.$$

The value for A_{FB} is in agreement with the predictions from the various models and shows that the $b \to c$ transitions are left chiral. The ARGUS update on α is in agreement with previous measurements [20].

3.4 Determination of $|V_{cb}|$

From our measurement of $\mathrm{Br}(\overline{B}^0 \to D^{*+}\,\ell^-\,\bar{\nu}) = (5.2 \pm 0.5 \pm 0.6)\%$ and an average lifetime $\tau_B = (1.32 \pm 0.04 \pm 0.12)\,\mathrm{ps}$ [21] the Kobayashi-Maskawa matrix element $|V_{cb}|$ can be de-

termined. Using the models [5,8–12] mentioned above we obtain values in the range from 0.036 to 0.045 (see Tab. 4).

It has been argued in [22] that the observed model dependence in the $|V_{cb}|$ determination can be considerably reduced by a fit to the q^2 spectrum or, equivalently, to the y spectrum with

$$y = \frac{m_B^2 + m_{D^*}^2 - q^2}{2\, m_B\, m_{D^*}}.$$

The prediction from HQET is determined by one universal form factor, the Isgur-Wise function $\xi(y)$ with the normalization $\xi(1) = 1$. In the case of finite quark masses, corrections of order $1/m_Q$ must be applied. It has been shown [22] that, specifically for the decay $B \to D^* \ell \nu$, these corrections vanish at the point of zero recoil, $y = 1$.

The differential width for this decay is given in [22] as:

$$\frac{1}{\tau_{\overline{B}^0}} \cdot \frac{dB\tau(\overline{B}^0 \to D^{*+} \ell^- \overline{\nu})}{dy} = \frac{G_F^2}{48\pi^3} m_{D^*}^3 (m_B - m_{D^*})^2 \cdot 0.99^2 \cdot |V_{cb}|^2 \xi^2(y) \sqrt{y^2 - 1} \times \left[4y(y+1) \frac{1 - 2yr + r^2}{(1-r)^2} + (y+1)^2 \right], \quad (8)$$

with $r = m_{D^*}/m_B$. The measured spectrum $d\mathrm{Br}/dq^2$ is shown in Fig. 7 together with fits of formula (8) using the functional forms for $\xi(y)$ given in Tab. 5. The table also includes the fit results for $|V_{cb}|$ and the so called "charge radius" ρ. In Fig. 8 the $|V_{cb}| \cdot \xi(y)$ distribution is shown as derived from the q^2 spectrum using eq. (8). The values of $|V_{cb}|$ are determined by the intersection of the fitted functions $\xi(y)$ with the ordinate since $\xi(1) = 1$.

The values for $|V_{cb}|$ shown in Tab. 5 vary from 0.045 to 0.053 depending on the analytical form chosen for the Isgur-Wise function. Without further knowledge of this function, the theoretical uncertainty in the determination of $|V_{cb}|$ on the basis of HQET is of comparable size to that seen in the quark model calculations of form factors [5,8–12]. Furthermore, the statistical errors on $|V_{cb}|$ derived with HQET (Tab. 5) are considerably larger than those obtained using [5,8–12] (Tab. 4). The reason is that the HQET approach has one additional parameter, the charge radius ρ which determines the slope of $\xi(y)$ at $y = 1$. Thus, the $|V_{cb}|$ measurement using HQET is essentially determined by the data points with the lowest y values, where the statistical precision is poor.

4 Summary and Conclusions

We have obtained an improved measurement of the $\mathrm{Br}(\overline{B}^0 \to D^{*+} \ell^- \overline{\nu}) = (5.2 \pm 0.5 \pm 0.6)\%$. A significant signal for the decay $\overline{B} \to D^{**} \ell^- \overline{\nu}$ is observed. The previous measurement [20] of the D^{*+} polarization parameter α has been improved leading to a value of $1.1 \pm 0.2 \pm 0.4$. The angular analysis has been extended to the distribution of the decay angle of the virtual W^-, allowing for a test of the chirality assignment to the weak b to c transition.

The expected sign for the forward-backward asymmetry has been confirmed, with $A_{FB} = 0.20 \pm 0.08 \pm 0.06$. A value for $|V_{cb}|$ can be extracted from $\mathrm{Br}(\overline{B}^0 \to D^{*+} \ell^- \nu_\ell)$ with good statistical precision, but with a large model dependence. The alternative method of obtaining $|V_{cb}|$ by fitting the q^2 spectrum on the basis of HQET does not reduce the model dependence since the Isgur-Wise Function is essentially undetermined. Furthermore, this method has considerably larger statistical errors, since $|V_{cb}|$ is determined largely by data only in the region near q^2_{max}.

Acknowledgement

It is a pleasure to thank U.Djuanda, E.Konrad, E.Michel, and W.Reinsch for their competent technical help in running the experiment and processing the data. We thank Dr.H.Nesemann, B.Sarau, and the DORIS group for the excellent operation of the storage ring. The visiting groups wish to thank the DESY directorate for the support and kind hospitality extended to them.

We especially thank J. G. Körner for providing essential formulas and his kind interest in the needs of the experimentalist.

References

[1] H. Albrecht *et al.* (ARGUS Collab.), Phys. Lett. B197 (1987) 452

[2] M. Aguilar-Benitez *et al.* (Particle Data Group), Phys. Rev. D45 (1992) 1

[3] N. Isgur, Phys. Rev. D43 (1991) 810

[4] S. Balk, F. Hussain, J. G. Körner, G. Thompson, MZ-TH-92-22 (1992)

[5] P. Ball, HD-THEP-92-25, to appear in: 27th Rencontres de Moriond, Proceedings (1992)

[6] M. A. Shifman, M. B. Voloshin, Sov. J. Nucl. Phys. 45 (1987) 292 and 47 (1988) 511

[7] J.G. Körner, G.A. Schuler, Phys. Lett. B226 (1989) 185

[8] J.G. Körner, G.A. Schuler, Z. Phys. C38 (1988) 511

[9] M. Bauer, B. Stech, M. Wirbel, Z. Phys. C29 (1985) 637

[10] B. Grinstein, N. Isgur, D. Scora, M.B. Wise, Phys. Rev. D39 (1989) 799

[11] K. Hagiwara, A.D. Martin, M.F. Wade, Nucl. Phys. B327 (1989) 569

[12] J.M. Cline, G. Kramer, W.F. Palmer, Phys. Rev. D40 (1989) 793

[13] H. Albrecht *et al.* (ARGUS Collab.), Nucl. Instr. Meth. A275 (1989) 1

[14] R. Waldi, internal ARGUS note on the MOPEK event generator

[15] M. Bengtsson, T. Sjostrand *et al.*, Comput. Phys. Commun. 43 (1990) 367

[16] F. Butler (CLEO Collab.), CLNS 92/1143

[17] H. Albrecht *et al.* (ARGUS Collab.), Phys. Lett. B232 (1989) 398; H. Albrecht *et al.* (ARGUS Collab.), Phys. Lett. B221 (1989) 422; J. C. Anjos *et al.* (E691 Collab.), Phys. Rev. Lett. 62 (1989) 1717; P. Avery *et al.* (CLEO Collab.), Phys. Rev. D41 (1990) 774

[18] H. Albrecht *et al.* (ARGUS Collab.), DESY 92-029

[19] J. G. Körner, private communication

[20] H. Albrecht *et al.* (ARGUS Collab.), Phys. Lett. B219 (1989) 121

[21] W. B. Atwood, J. A. Jones, in S. Stone (editor) "B decays", 261, World Scientific Publishing Co. Pte. Ltd. (Singapore, New Jersey, London, Hong Kong) 1992

[22] M. Neubert, Phys. Lett. B264 (1991) 455; M. Neubert, SLAC-PUB-5826 (1992)

I	$\overline{B}^0 \to \overline{(D^{*+}\,\ell^-)}\,\overline{\nu}$
II	$\overline{B}^0 \to D^{**+}\,\overline{(\ell^-}$ $\hookrightarrow\ \overline{D^{*+})}\ \overline{\nu}\ \pi^0$ $\quad B^- \to D^{**0}\,\overline{(\ell^-}$ $\hookrightarrow\ \overline{D^{*+})}\ \overline{\nu}\ \pi^-$
III	$B_1 \to \overline{(\ell^-}\ \overline{D^{*+})}\ X_1$ $B_2 \to \overline{(\ell^-}\ \overline{D^{*+})}\ X_2$
IV	$e^+e^- \to c\bar{c} \to \overline{(D^{*+}\,\ell^-)}\ X$

Table 1: The four event classes considered as signal (I) and background (II to IV) processes.

Result for:	Data: $K\pi$	$K3\pi$	$K\pi + K3\pi$
I	114±13±6	124±23±9	235±24±11
II	34± 9±2	21±13±4	63±15± 6
III	8± 4±5	14±10±6	16± 7± 8
IV	7± 4±1	6± 9±1	13± 7± 5
$\frac{N(D^{**}\ell^-)}{N(D^{*+}\ell^-)}$	0.30±0.10±0.03	0.18±0.12±0.05	0.27±0.08±0.03
$\mathrm{Br}(\overline{B}^0 \to D^{*+}\,\ell^-\,\overline{\nu})[\%]$	5.5±0.6±0.7	4.7±0.9±0.5	5.2±0.5±0.6
α	1.05±0.48±0.18	1.14±0.70±0.38	1.12±0.39±0.19
A_{FB}	0.14±0.10±0.06	0.27±0.12±0.06	0.20±0.08±0.06

Table 2: Results from the simultaneous fit of the measured $\Delta N/\Delta M^2_{rec}$, $\Delta N'/\Delta\cos\theta$, $\Delta N'/\Delta\cos\theta^*$, and $\Delta N'/\Delta q^2$.

i	type of D^{**}	$\mathrm{Br}(D_i^{**+} \to D^* X)$	$\frac{\mathrm{Br}(\overline{B}^0 \to D_i^{**+} \ell^- \bar{\nu})}{\mathrm{Br}(\overline{B}^0 \to D^{**+} \ell^- \bar{\nu})}$	ϵ_i^{**}	
			GISW	GISW	BHKT
1	$D(1^1P_1)$	1	0.41	0.76	0.83
2	$D(1^3P_0)$	0	0.11	0.00	0.00
3	$D(1^3P_1)$	1	0.21	0.48	0.81
4	$D(1^3P_2)$	1/4 [17]	0.14	0.73	0.75
5	$D(2^1S_0)$	1	0.07	0.66	0.63
6	$D(2^3S_1)$	3/4	0.06	0.70	0.60

Table 3: Various branching ratios and relative efficiencies ϵ_i^{**} needed for the estimation of $\frac{\mathrm{Br}(\overline{B}^0 \to D^{**+} \ell^- \bar{\nu})}{\mathrm{Br}(\overline{B}^0 \to D^{*+} \ell^- \bar{\nu})}$ from the visible ratio $\frac{N(D^{**} l)}{N(D^* l)}$

	$\lvert V_{cb}\rvert \times 10^3$
PB [5]	$45 \pm 2 \pm 3$
KS [8]	$39 \pm 2 \pm 2$
BSW [9]	$39 \pm 2 \pm 2$
GISW [10]	$40 \pm 2 \pm 2$
HMW [11]	$39 \pm 2 \pm 2$
CKP [12]	$36 \pm 2 \pm 2$

Table 4: Results on $|V_{cb}|$ calculated from our value for $\mathrm{Br}(\overline{B}^0 \to D^{*+} \ell^- \bar{\nu})$ for various theoretical models.

	$\xi(y)$	$\lvert V_{cb}\rvert \times 10^3$	ρ	χ^2/df
A	$1 - \rho^2(y-1)$	$45 \pm 5 \pm 3$	$1.08 \pm 0.11 \pm 0.03$	5.1/6
B	$\frac{2}{y+1} \exp\left[-(2\rho^2 - 1)\frac{y-1}{y+1}\right]$	$53 \pm 8 \pm 3$	$1.52 \pm 0.21 \pm 0.10$	4.3/6
C	$\left(\frac{2}{y+1}\right)^{2\rho^2}$	$51 \pm 8 \pm 3$	$1.45 \pm 0.19 \pm 0.09$	4.3/6
D	$\exp\left[-\rho^2(y-1)\right]$	$50 \pm 8 \pm 2$	$1.37 \pm 0.19 \pm 0.08$	4.4/6

Table 5: Results on $|V_{cb}|$ and the "charge radius" ρ from various parametrizations of the Isgur-Wise-function $\xi(y)$ [22] for fitting the q^2-distribution

Figure Captions

Fig. 1 Definition of the polar angles θ and θ^* and azimutal angle χ.

Fig. 2 Invariant mass of $(D^0\,\pi^+)$ combinations with (a) $D^0 \to K^-\,\pi^+$ and (b) $D^0 \to K^-\,\pi^+\,\pi^+\,\pi^-$, for events containing either an e^- or μ^- with momentum larger than $1\,\mathrm{GeV}/c$.

Fig. 3 The M^2_{rec} distributions expected for processes I to IV listed in Tab. 1, arbitrarily normalized to unit area.

Fig. 4 Measured M^2_{rec} distributions (points with error bars) for the two D^0 decay channels, fitted by a linear combination of the curves shown in Fig. 3. The blank and shaded areas correspond to the rates for the signal process (I) and the feeddown process (II), respectively. The continuum process (IV) is shown as dashed line.

Fig. 5 Measured distribution of the invariant $(D^{*+}\,\pi^-)$ mass (points with error bars) obtained for $M^2_{rec} > 0$. The dashed histogram was obtained for $M^2_{rec} < 0$ and has been scaled to describe the combinatorial background in the distribution for $M^2_{rec} > 0$. The dotted curve describes the background function fitted to the dashed histogram, whereas the solid line is the sum of the background function and two Breit-Wigner curves at masses of $2420\,\mathrm{GeV}/c^2$ and $2460\,\mathrm{GeV}/c^2$ fitted to the distribution with error bars.

Fig. 6 The measured $\cos\theta$, $\cos\theta^*$, M^2_{rec}, and q^2 distributions, uncorrected for efficiency. The solid line histograms are the fitted sums of Monte Carlo distributions expected for the four processes I – IV. The shaded histograms show the amount and shape of the background due to process $\overline{B} \to D^{**}(2420)\,\ell^-\,\overline{\nu}$.

Fig. 7 q^2-distribution of the decay $\overline{B}^0 \to D^{*+}\,\ell^-\,\overline{\nu}$ corrected for background and efficiency. The four lines correspond to the fit of formula (8) and the four analytical expressions for the Isgur-Wise Function of Tab. 5. The dotted line corresponds to $\xi(y) = 1 - \rho^2(y-1)$.

Fig. 8 Measured distribution $\Delta\mathrm{Br}(\overline{B}^0 \to D^{*+}\,\ell^-\,\overline{\nu})/\Delta y$ transformed to correspond to $|V_{cb}|\cdot\xi(y)$. The four lines represent the four analytical expressions for the Isgur-Wise Function of charge radius ρ times $|V_{cb}|$ of Tab. 5. The dotted line corresponds to $\xi(y) = 1 - \rho^2(y-1)$.

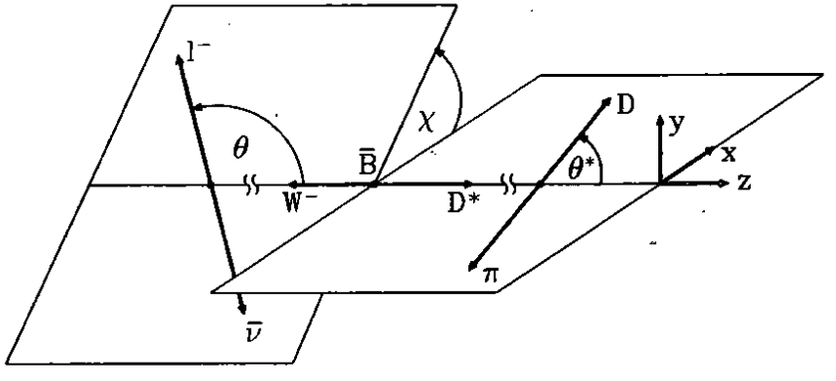

Figure 1

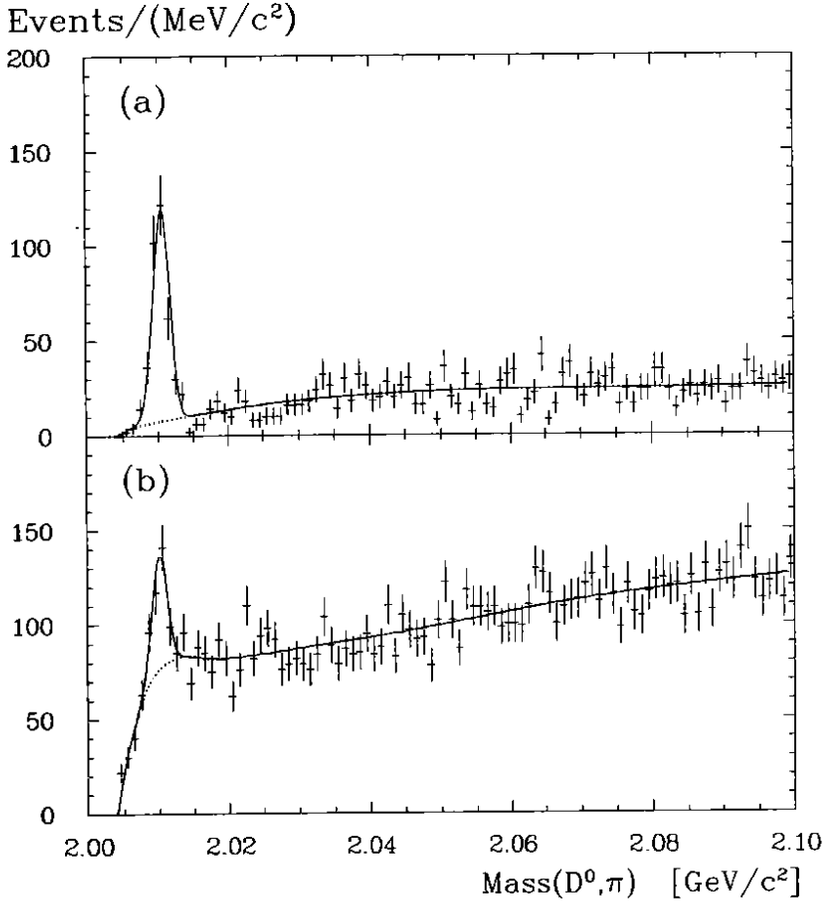

Figure 2

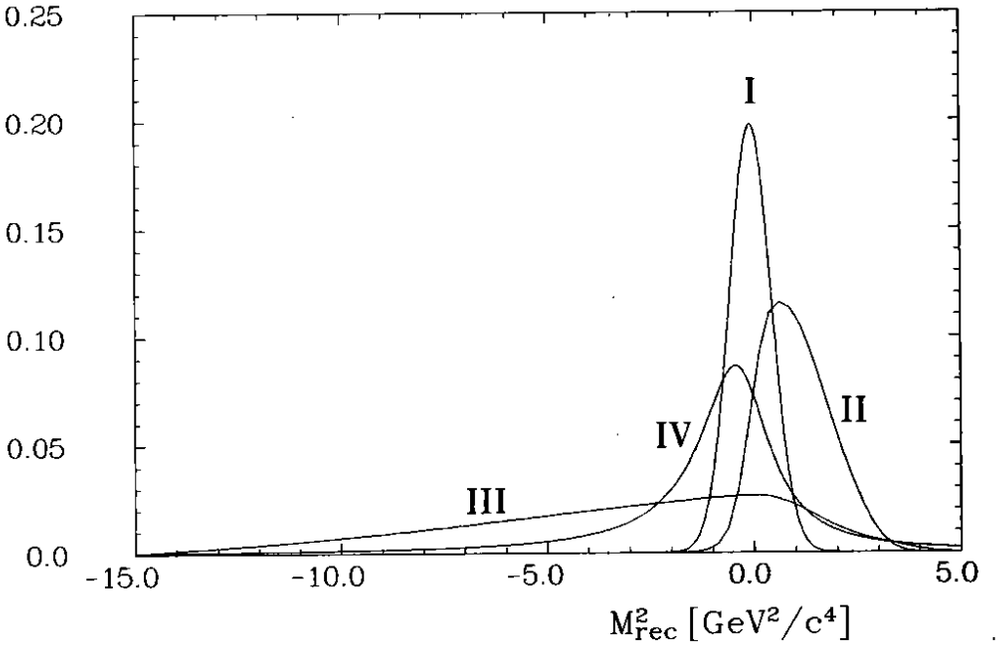

Figure 3

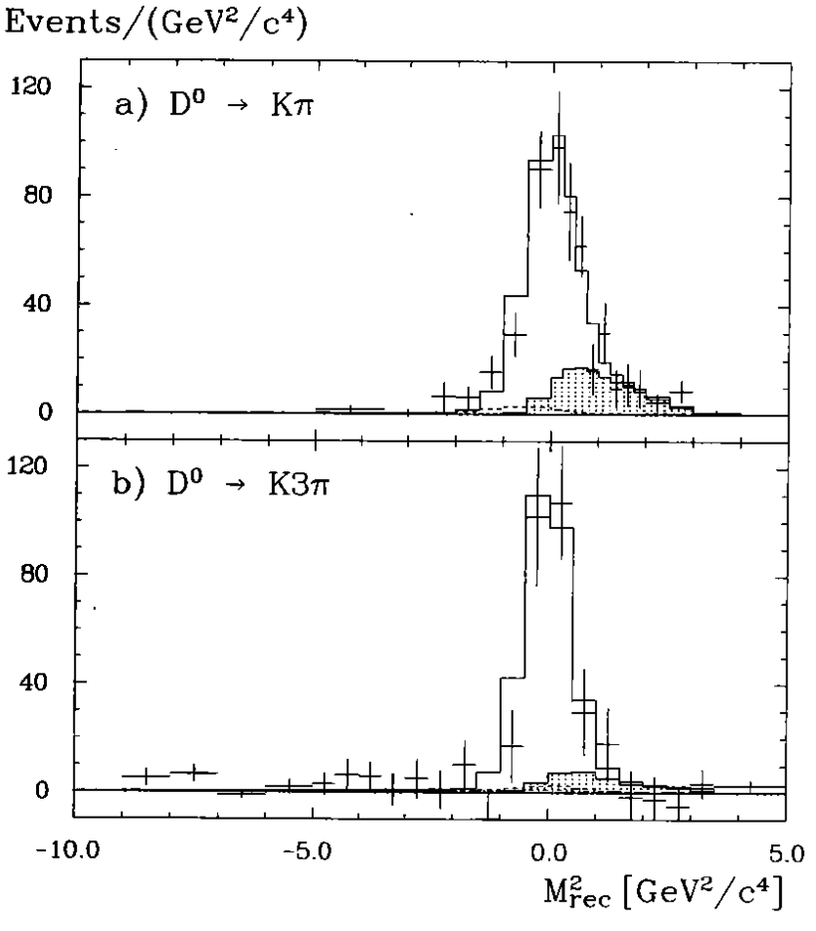

Figure 4

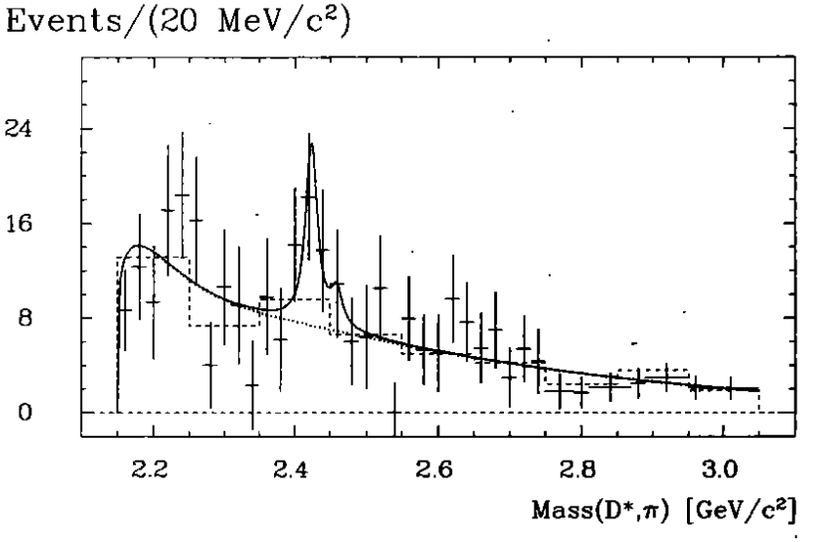

Figure 5

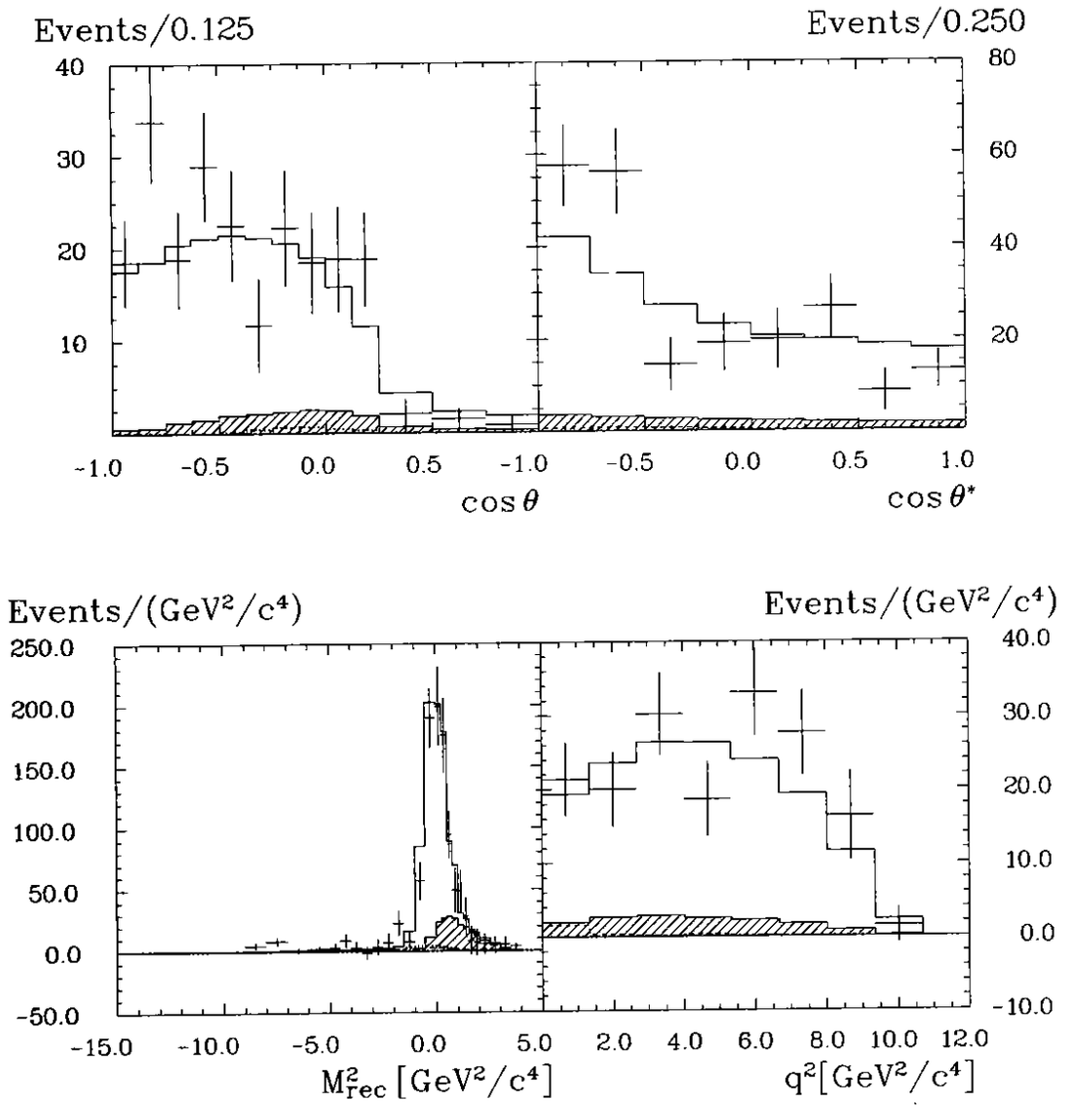

Figure 6

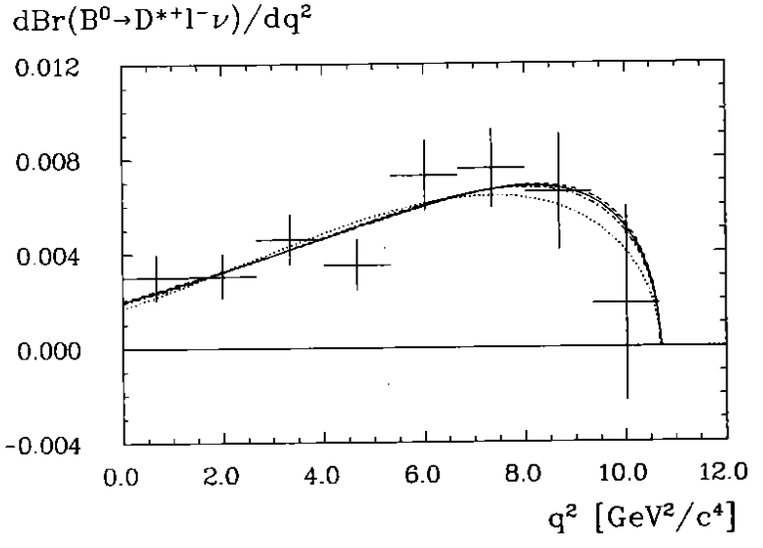

Figure 7

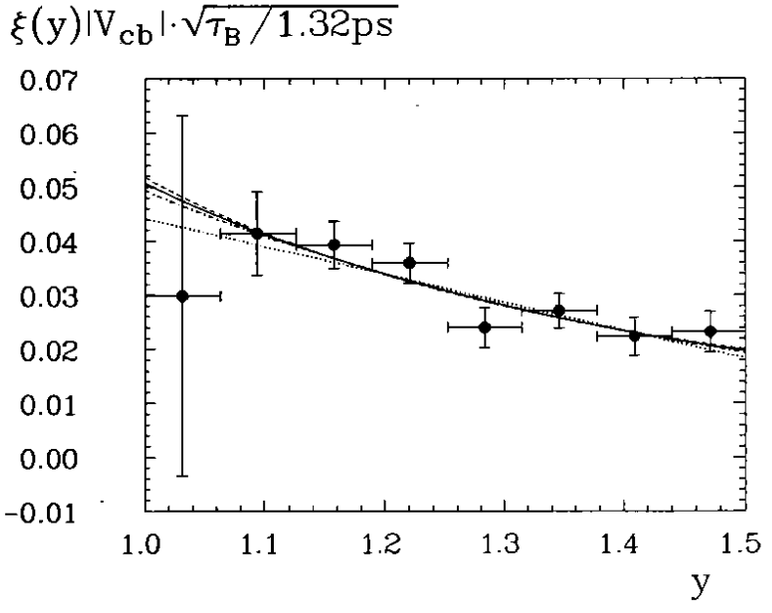
$\xi(y)|V_{cb}|\cdot\sqrt{\tau_B/1.32ps}$
0.07
0.06
0.05
0.04
0.03
0.02
0.01
0.00
-0.01
1.0
1.1
1.2
1.3
1.4
1.5
y

Figure 8